13th International Workshop on Innovative Simulation for Healthcare, 012
21st International Multidisciplinary Modeling & Simulation Multiconference

2724-0371 © 2024 The Authors.
doi: 10.46354/i3m.2024.iwish.012

Molecular docking of triazole-based ligands with KDM5A to identify potential inhibitors

Jose Siguenza[1,*] and Haci Baykara[2]

[1]Center of Nanotechnology Research and Development (CIDNA), Campus Gustavo Galindo Km 30.5 Vía Perimetral, Guayaquil, 090506, Ecuador
[2] Facultad de Ingeniería Mecánica y Ciencias de la Producción, Campus Gustavo Galindo Km 30.5 Vía Perimetral, Guayaquil, 090506, Ecuador

[*]Corresponding author. Email address: jasiguen@espol.edu.ec

Abstract

KDM5A, implicated in diverse cancer types, including breast cancer, serves as a crucial regulator of tumor progression, metastasis, and drug resistance. As a histone demethylase, targeting KDM5A presents a promising therapeutic strategy. We used a library of 61,612 compounds, some of which were triazole-like ligands, to generate binding poses targeting the KDM5A catalytic pocket. Different chemoinformatic and bioinformatic techniques were used, such as molecular fingerprints, Tanimoto similarity, and Autodock Vina through Deepchem. Triazole derivatives 700, 91, and 449 were the best at inhibiting KDM5A demethylase activity. It was found that compound 700 had a stronger binding affinity for KDM5A and lower IC50 values, at -11.042 kcal/mol and 0.01 M, compared to doxorubicin, a well-known breast cancer inhibitor. Furthermore, triazole compounds 91 and 499 demonstrated promising potential as KDM5A inhibitors. This study of triazole-like molecules for virtual screening suggests a workflow to identify triazole derivative drugs that are selective for KDM5A-type cancer.

Keywords: Triazole derivatives; molecular docking; KDM5A; virtual screening

1. Introduction

An increase in genetic changes that interfere with regular cellular functions and control systems, resulting in abnormal and varied cell growth, is what leads to the development of cancer (Elmorsy et al., 2023). Cancer can be caused by various factors, such as genetics, environmental exposures, and molecular-level changes (Schmitt and Greten). This complexity makes it challenging to understand the mechanisms of cancer and develop targeted treatments. Molecular docking has emerged as a computer-based technique facilitating the identification and optimization of potential therapeutic agents (Eberhardt et al., 2021; Friesner et al., 2004). As discussed in numerous studies, molecular docking is effective in predicting the binding affinity and orientation of small molecules to target proteins (Yang et al., 2019; Li et al., 2024). Molecular docking and high-throughput screening have made it faster to find new drugs that stop proteins like kinases, proteases, and receptor tyrosine kinases that cause cancer (Jurutka et al., 2021).

It is an enzyme that is part of a group of histone demethylases called Jumonji C (JmjC) (Jose et al., 2020). It is also known as Lysine Demethylase 5A or JARID1A. This enzyme removes tri- and di-methylated lysine 4 from histone H3 (H3K4me3 and H3K4me2) (Horton et al., 2016). Since this change is usually linked to active gene transcription, KDM5A is very important for controlling gene expression because it removes these activating marks and helps stop transcription. By demethylating H3K4me3/2, KDM5A

acts to repress the transcription of various genes. KDM5A is often overexpressed in several types of cancer, including breast, prostate, and lung cancers, leading to aberrant gene repression and contributing to tumor growth, metastasis, and resistance to therapy (Ortiz et al., 2023; Yang et al., 2019). KDM5A-N8 (PDB ID: 5ive) is designed to inhibit the enzymatic activity of KDM5A by targeting the histone demethylase KDM5A (also known as JARID1A or RBP2) (Horton et al., 2016). N8 inhibitor stops the removal of methyl groups from H3K4 by blocking KDM5A. Given the role of KDM5A in cancer, KDM5A-N8 has potential as a therapeutic agent. Inhibiting KDM5A could reactivate tumor suppressor genes and other critical regulatory genes that are otherwise repressed in cancer cells.

Triazole compounds have shown significant potential in cancer therapy due to their ability to inhibit critical enzymes and disrupt cancer cell proliferation pathways (Kumar et al., 2024; Avula et al., 2023). In particular, these chemicals have been successful at targeting proteins that play a role in epigenetic regulation, like histone demethylases, which are important in the growth of many types of cancer (Yang et al., 2019; Kumar et al., 2024). This study investigates whether triazole-like molecules, when docked to the KDM5A enzyme using molecular docking techniques, can act as effective enzyme inhibitors. This inhibition could disrupt KDM5A's role in controlling epigenetic modifications, thereby impeding cancer progression.

1.1. Molecular Docking State of the Art

Molecular docking has advanced significantly, becoming a cornerstone technique in drug discovery and structural biology. By 2023, the incorporation of artificial intelligence (AI) and machine learning (ML) will have notably improved the prediction accuracy of molecular interactions (Corso et al., 2022). Modern docking tools like AutoDock Vina and Glide have better scoring functions and more adaptative docking protocols, considering solvent effects and flexible proteins (Eberhardt et al., 2021; Friesner et al., 2004). These tools have significantly increased the efficiency of virtual screening processes, enabling the rapid identification of potential drug candidates (Sliwoski et al., 2014). The use of protein structure prediction tools such as AlphaFold has provided high-quality templates that enhance docking studies (Jumper et al., 2021). This improvement has made molecular docking more useful by letting scientists look at targets that they could not before and making it easier to find new binding and allosteric sites (Senior et al., 2020). Such capabilities are crucial for the development of targeted therapies and for understanding complex biological systems.

The accuracy of docking predictions has also been improved by combining molecular docking with high-throughput experimental methods such as cryo-EM and X-ray crystallography. These experiments give us detailed information about the structures of molecules that, when put together with computer docking, give us a full picture of how molecules interact with each other. This synergy has made it possible to study large and complex protein assemblies, thus accelerating the drug discovery process and improving the design and optimization of therapeutic compounds (Gorgulla et al., 2020). Consequently, molecular docking continues to be a powerful tool in modern biomedical research, significantly contributing to the development of new drugs and therapeutic strategies. In addition to advancements in molecular docking technology, significant progress has been made in understanding specific molecular targets such as KDM5A (Lysine Demethylase 5A). New research has focused on creating selective inhibitors for KDM5A using cutting-edge docking methods to find out where it binds and how it works (Jose et al., 2020).

Autodock Vina through Deepchem was used in this study to check how well KDM5A binds to a set of triazole derivatives chosen from a larger dataset; more details about this are in Section 2. Research on KDM5A highlights the critical role of molecular docking in modern drug discovery, showcasing how computational tools can accelerate the identification and optimization of therapeutic agents. Several studies are being made to treat cancers that are linked to abnormal histone methylation using state-of-the-art methods (Horton et al., 2016; Jose et al., 2020). Even though the present study does not include experimental methods or technologies such as AlphaFold's structure prediction, we propose and expand more studies in discussion in Section 3.

2. Materials and Methods

In molecular docking, both protein and ligand structures are crucial to running a successful and reliable simulation. To properly prepare a protein, structural errors must be fixed, missing atoms must be added, and the right protonation states must be assigned. These modifications are necessary for a realistic representation of the binding site. Ligands also need a preparation step, but before preparing the ligands, we selected triazole-like compounds from the ligand dataset. Then, we prepared molecules by optimizing the geometry, assigning the correct charges, and ensuring that the tautomeric and ionization states were accurate, which are crucial for correct interaction prediction. When these files were prepared, molecular docking was conducted safely. Figure 1 illustrates the main workflow we used in this study.

2.1. Protein and Ligand Datasets

2.1.1. KDM5A Co-Crystal Structure

KDM5A-linked Jumonji domain crystal structures are available in Protein Data Bank databases (Horton et al.). Figure 2 represents KDM5A-N8 (PDB ID: 5ive) which was the target for molecular docking.

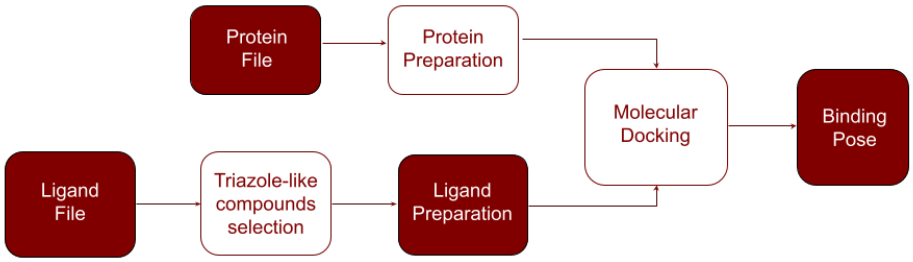

Figure 1. Molecular docking workflow used in this study, including triazole-like selection of compound from the enamine premium dataset

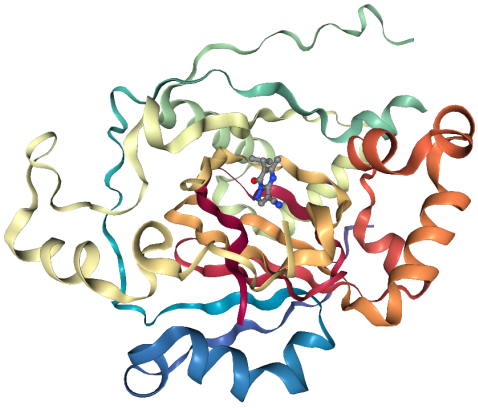

Figure 2. Co-crystal structure of KDM5A and N8 inhibitor (PDB ID: 5ive)

2.1.2. *Enamine Screening Collection*

The enamine screening dataset comprises diverse chemical compounds designed for virtual screening and drug discovery purposes. We use the premium collection, a subset of the screening collection, of 61,612 synthesized compounds (Ltd2023). The premium enamine dataset has compounds that have the best physical and chemical properties, such as Fsp3, low LogP, and low molecular weight (about 350 g/mol on average).

2.2. Software requirements and dependencies

For the data preparation and docking simulations, we used an Intel (R) Xeon (R) CPU @ 2.20 GHz with 2 vCPUs and 13 GB of RAM provided by Google Collaboratory (Colab) (Nelson and Hoover, 2020). As the main programming language, we used Python 3.10.12 (Van Rossum and Drake Jr, 1995). OpenBabel and OpenMM libraries were used to remove N8 inhibitor heteroatoms present in the protein file. Hydrogens were added, 3D conformers were made, and the best geometry for ligands was found (Eastman et al., 2017; O'Boyle et al., 2011). Docking simulations were conducted using AutoDock Vina and Deepchem functions to manage file type conversions and define docking parameters (Eberhardt et al., 2021; Ramsundar et al., 2019). Autodock Vina uses an exhaustiveness parameter, which is directly related to vCPU availability. For this reason, we set exhaustiveness to two and generate 1 number of modes. These arguments were passed directly to Deepchem's *VinaPoseGenerator* object. In addition, RDKit was employed to select triazole-like ligands and visualize the ligand's structure (RDKit, online).

2.3. Select triazole-like molecules

Triazoles are five-membered heterocyclic compounds containing three nitrogen atoms and two carbon atoms. Triazoles can exist in two isomeric forms, presented in Figure 3, 1,2,3-triazole, and 1,2,4-triazole, depending on the positions of the nitrogen atoms within the ring.

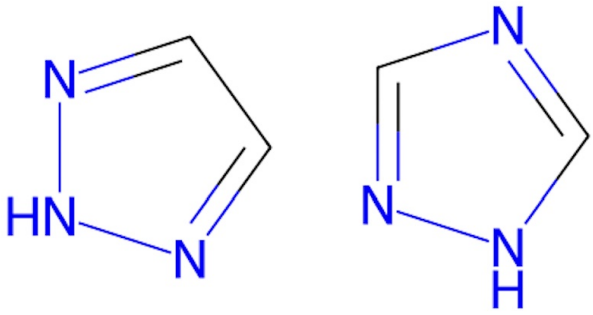

Figure 3. From right to left, 1, 2, 3-Triazole and 1, 2, 4-Triazole

2.3.1. *Molecular fingerprints*

In RDKit, molecular fingerprints are typically binary vectors that encode the presence or absence of particular molecular substructures. In this study, we use Morgan fingerprints in RDKit, which are a type of circular fingerprints used to represent molecular structures (triazole in this case) as binary vectors. Figure 4 represents triazole fingerprints represented as molecular fragments. These fingerprints capture the presence of circular substructures centered around each atom within the molecule. For triazole molecules, Morgan's fingerprints would encode the connectivity and surroundings of each atom in the ring. By specifying a radius, the fingerprinting process considers the atom and its neighbors up to that radius. We set a radius of 2, which would account for the atom itself and its neighbors up to two bonds away. This method records triazole's structural features, which lets us make a binary vector representation that can be used for many

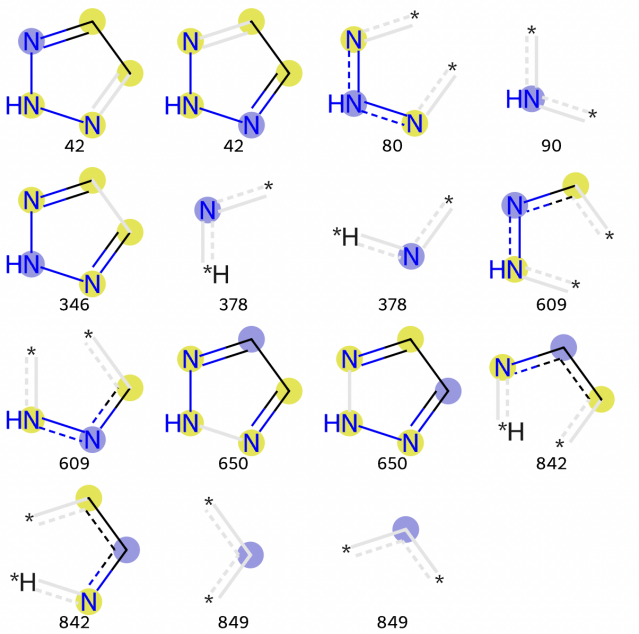

Figure 4. Triazole molecular fingerprints using Morgan fingerprints with a radius of 2 units. In this case, indices 42, 80, 90, 346, 378, 609 650, 832, and 849 are one value from the bit vector, which means the existence of a molecular fragment

computer tasks, like finding similarities, clustering, and studying the relationship between structure and activity. The resulting binary vector highlights the specific circular substructures present in triazole.

2.3.2. *Tanimoto similarity*

RDKit's Tanimoto similarity is a metric used to compare the similarity between two molecular fingerprints. The Tanimoto similarity coefficient is calculated as the ratio of the intersection to the union of the fingerprint sets:

$$Tanimoto\ similarity = \frac{c}{a + b - c} \quad (1)$$

where,

- a is the number of bits set to 1 in the first fingerprint,
- b is the number of bits set to 1 in the second fingerprint,
- c is the number of bits set to 1 in both fingerprints (the intersection).

The Tanimoto similarity ranges from 0 to 1, where 0 indicates no similarity and 1 indicates identical fingerprints. We set a cutoff of 0.1 for Tanimoto similarity to broaden the docking search space.

2.4. Protein and Ligand Preparation Methodology

2.4.1. *Protein Cleaning*

The N8 inhibitor needs to be removed from the 5IVE file to run an appropriate docking simulation. Also, we added hydrogens at pH 7, including missing heavy atoms.

2.4.2. *Ligand Preparation*

Ligands from the enamine premium collection are shown as 2D shapes, but to show how proteins interact with ligands, 3D structures are needed. OpenBabel was used for generating 3D conformers, adding missing hydrogens, and minimizing the structure's energy.

2.5. Visualization tools

NGLViewer was used to visualize the 3D molecular structures (i.e., KDM5A, ligands, and protein-ligand complexes) (Rose et al.). RDKit was used to generate Simplified Molecular Input Line Entry System (SMILES) and kekulize structures for top-score ligands and Matplotlib to plot scores distribution (Hunter, 2007).

3. Results and Discussion

As part of our virtual screening of triazole-like compounds, we ran a blind docking simulation using the whole protein structure for docking. From the enamine premium collection, 3.85% of the compounds were selected as triazole-like compounds by applying molecular fingerprints and comparing them with Tanimoto similarity. This means that, setting a Tanimoto similarity of 10%, 2 411 ligands were used for molecular docking simulations. However, not all the ligands selected were triazole derivatives. Tanimoto's metric considers molecular fingerprints, some of which are not unique to triazole compounds. This included azoles, and cyclic compounds containing at least one nitrogen atom. Figure 5 presents a normal distribution of Autodock Vina scores for binding poses, ranging from -3.42 kcal/mol to the highest and lowest of -11.04 kcal/mol.

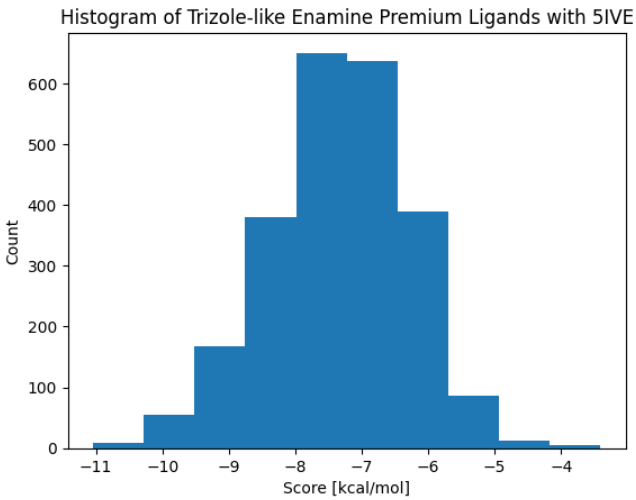

Figure 5. Histogram of triazole-like enamine premium ligands with 5ive

Table 1. Autodock Vina scores, IC50 values and smile representations of top 40 triazole derivatives and doxorubicin binding poses .

Ligand No	Autodock Vina Scores $\left[\frac{kcal}{mol}\right]$	IC50 [μM]	SMILES
700	−11.042	0.01	O=C(c1cccc2ncnn12)N1CC2(CCCCC2)[C@@H]1c1ccccc1
91	−10.658	0.02	COc1ccc2cccc(CC(=O)N3CCn4c(nnc4-c4cccnc4)C3)c2c1
449	−10.261	0.03	O=C(Nc1ccccc1Cn1cncn1)N1CC2(CCC2)[C@H]1c1ccccc1
284	−9.985	0.05	Cn1cnnc1C[C@]1(O)CCCN(Cc2ccc3c(c2)CCCC3)C1
1021	−9.877	0.06	CC(C)c1nnc2n1C[C@@H](NC(=O)N1CCCn3c(cc4ccccc43)C1)CC2
624	−9.847	0.06	Cn1cnn(-c2ccc(NC(=O)N3CC4(CCC4)[C@H]3c3ccccc3)cc2)c1=O
344	−9.802	0.07	O=C(Nc1cccc(-n2ccnn2)c1)N[C@H]1c2ccccc2CC12CCOCC2
1178	−9.735	0.07	Cc1nnc2n1C[C@@H](C(N)=O)N(C(=O)Cc1ccc3c(c1)CCC3)C2
785	−9.554	0.1	O=C(NCc1nnc(-c2ccncc2)[nH]1)N1CC2(CCCC2)c2cccc(F)c21
65	−9.543	0.1	Cc1nnc([C@H]2OCC[C@H]2CNC(=O)c2cccc3c(C)c(C)[nH]c23)[nH]1
1322	−9.527	0.1	O=C(c1ccc(Oc2ccccc2)cn1)N1CCn2c(nnc2-c2cccnc2)C1
1164	−9.436	0.12	Cc1nnc2n1C[C@@H](C(N)=O)N(C(=O)c1ccc3c(c1)CCC=C3)C2
823	−9.359	0.14	CC(C)n1ncnc1NC(=O)N1C[C@H](c2ccccc2)[C@H]2COCC[C@@H]21
1441	−9.218	0.17	O=C(c1cn([C@@H]2COC[C@H]2O)nn1)N1CCc2ccccc2C1
1323	−9.197	0.18	Cc1nnc([C@H]2OCC[C@H]2CNC(=O)Cc2c(C)[nH]c3ccccc23)[nH]1
442	−9.171	0.19	O=S(=O)(Cc1nnc2n1CCCCC2)c1nc(-c2ccc3c(c2)CCC3)n[nH]1
1008	−9.049	0.23	Cn1cnnc1C[C@]1(O)CCCN(c2nc3ccccc3cc2CO)C1
776	−8.982	0.26	CCc1ccc([C@@H]2CN(c3cc4nncn4c(C)n3)CCO2)cc1
290	−8.972	0.26	CCn1ncnc1CNC(=O)N1C[C@H](c2ccccc2)[C@H]2COCC[C@@H]21
1077	−8.956	0.27	Cc1nnc([C@H]2OCC[C@H]2CNc2nc3c(cc2CN)CCCC3)[nH]1
152	−8.926	0.29	CO[C@@H]1C[C@@H](c2nnc3n2CCC3)N(Cc2ccc3ccccc3n2)C1
1475	−8.917	0.29	Cc1cc(F)cc2c1CN(C(=O)c1cn([C@@H]3COC[C@H]3O)nn1)CC2
1158	−8.905	0.3	Cc1ccc(C(=O)N2Cc3nnc(C)n3C[C@H]2C(N)=O)c2c1CCC2
752	−8.886	0.31	CCn1nncc1C(=O)N1CC2(CCCC2)c2cccc(Cl)c21
701	−8.885	0.31	O=C(c1cccn2c(=O)[nH]nc12)N1CC2(CCCCC2)[C@@H]1c1ccccc1
1070	−8.867	0.32	O=C(N[C@@H]1c2ccccc2C[C@@H]1O)c1nc2n(n1)CCCN2
1162	−8.865	0.32	Cc1nnc2n1C[C@@H](C(N)=O)N(C(=O)c1cccc(C3CCC3)c1)C2
222	−8.833	0.33	Cn1cc([C@@H]2CS(=O)(=O)CCN2Cc2ncnn2-c2ccccc2)cn1
2361	−8.807	0.35	Cc1c(C(=O)N(C)C[C@H]2OCC[C@H]2c2ncn[nH]2)oc2ccccc12
1069	−8.798	0.36	O=C(N[C@@H]1c2ccccc2C[C@@H]1O)c1nc2n(n1)CCCN2
164	−8.793	0.36	CO[C@@H]1C[C@@H](c2nnc3n2CCC3)N(C(=O)Cc2cc(C)ccc2C)C1
352	−8.775	0.37	Cc1nc2n(n1)C[C@@H](NC(=O)N1CCC(c3noc4cc(F)ccc34)CC1)CC2
787	−8.767	0.37	Cc1cc(F)ccc1C1CCN(C(=O)NCc2nnc(-c3ccncc3)[nH]2)CC1
1016	−8.765	0.38	Cn1cnnc1C[C@]1(O)CCCN(Cc2ccc3occc3c2)C1
1483	−8.751	0.38	O=C(c1cn([C@@H]2COC[C@H]2O)nn1)N1Cc2cccc(Cl)c2C1
1474	−8.724	0.4	Cc1cc(F)cc2c1CN(C(=O)c1cn([C@@H]3COC[C@H]3O)nn1)CC2
73	−8.695	0.42	Cn1c([C@@H]2Cc3ccccc3O2)nnc1N1CC[C@@]2(CNC(=O)C2)C1
1791	−8.684	0.43	CO[C@@H]1C[C@H](c2ncc[nH]2)N(C(=O)c2cccc(-c3ncn[nH]3)c2)C1
738	−8.678	0.43	CCC1(c2ccccc2)CN(C(=O)Nc2ccc(-n3ccnn3)cc2)C1
1013	−8.677	0.44	Cn1cnnc1C[C@]1(O)CCCN(Cc2ccc3c(c2)CCO3)C1
2355	−8.671	0.44	Cc1ccc2[nH]c(C(=O)N(C)C[C@H]3OCC[C@H]3c3ncn[nH]3)cc2c1C
Doxorubicin	**-7.59**	**2.72**	**Cc1[nH]c2c(CN)cnn2c(=O)c1C(C)C**

In the scope of this study, the lowest triazole derivative molecules were selected after performing molecular docking. Also, we include doxorubicin, which is an approved drug targeting breast cancer, in docking simulations as a control experiment. Table 1 showcases the lowest estimated binding free energies, IC50 values, and SMILES representations. Doxorubicin results are similar to reports from relative studies (Elmorsy et al., 2023; Avula et al., 2023).

AutoDock Vina predicts bound conformations and scores that indicate binding affinity. NGL Viewer was used to create three-dimensional visualizations to analyze and illustrate the interactions between the KDM5A protein residues ligand 700, presented in Figure 6. In the predicted conformation, the binding pocket of 700 included three key residues: Cys481, Tyr472, and Lys501. In particular, forming hydrogen bonds with Lys501 and Cys481 and pi-bond with Tyr472. According to AutoDock Vina scores in Table 1, ligand 700, with a score of −11.042 kcal/mol, was the most potent compound. Ligands 91, 449, 284, 1021, 624, and 344 had scores of −10.658 kcal/mol, −10.261 kcal/mol, −9.985 kcal/mol, −9.877 kcal/mol, −9.847 kcal/mol, and −9.802 kcal/mol, respectively (Table 1). The lower AutoDock Vina scores for ligands 700, 91, and 449 prompted the synthesis of these compounds for further biological evaluation. The triazole derivative compounds in Table 1 bind to the active site in the KDM5A-N8 co-crystal structure in a way that is similar to what was seen before. Figure 7 shows triazole derivative structures for 700, 91, and 449.

Even though these results are not conclusive enough to claim new chemotherapeutic agents, Autodock Vina scores of 700, 91, and 449 suggest a strong affinity to inhibit KDM5A. In terms of molecular docking computation

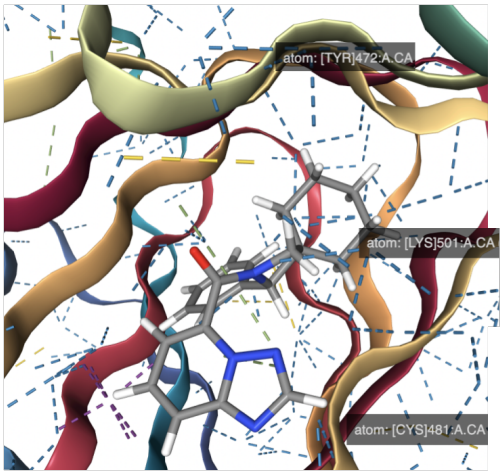

Figure 6. 3D binding pose between 700 and 5ive's active site, including interatomic interactions

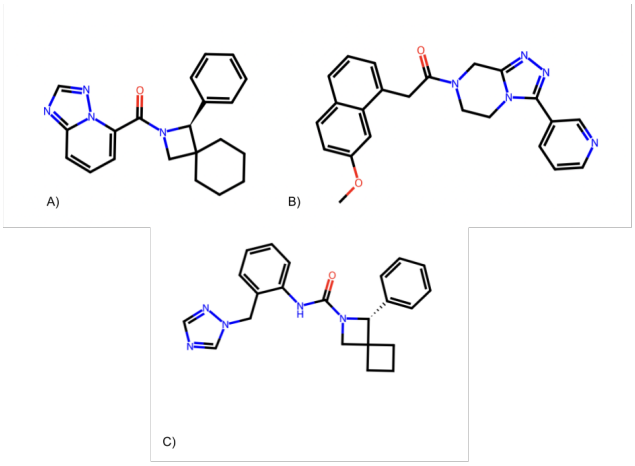

Figure 7. Top scoring triazole derivative compounds after molecular docking simulations. A) 700, B) 91, C) 449

requirements, increasing virtual CPUs and exhaustiveness can lead to new binding conformations. We recommend synthesizing these compounds and conducting additional experimental analyses such as apoptosis assays, MTT assays, ADME studies, X-ray crystallography, and Cryo-EM to evaluate their medicinal properties since these compounds possess the potential to be better candidates that exhibit promising IC50 profiles for further study. This detailed structural information from the docking study helps in designing or modifying compounds with better affinity and selectivity in the future. Also, it would be interesting to apply structure prediction strategies such as alphafold and target new structures.

4. Conclusions

We chose 2,411 triazole-like ligands from the Enamine Premium database, which has 62,612 compounds. Then, we used Autodock Vina and Deepchem software to do molecular docking simulations against KDM5A (PDB ID: 5ive). Among these newly identified inhibitor candidates, compounds 700, 91, and 449 exhibited the lowest Autodock Vina scores (< -10 kcal/mol). Compound 700 displayed the lowest score at -11.042 kcal/mol, with an estimated IC50 value of approximately 0.01 μM. Triazoles 91 and 449 demonstrated comparable IC50 values of 0.02 and 0.03 μM, respectively. Notably, the docking score of the well-established agent doxorubicin was in agreement with its IC50 experimental value, with a score of -7.59 kcal/mol and an IC50 value of 2.72 μM. The binding energy score of the triazole derivatives, which resulted from hydrogen bonds and π−H interactions with the protein residues, followed the order of 700 < 91 < 449, with scores of -11.042, -10.658, and -10.261, respectively. Finally, the top triazole derivatives (700, 91, and 449) presented low IC50 values, making them potential therapeutic agents, but further analysis, such as experimental methods and the application of state-of-the-art methods, should be addressed in future studies.

5. Funding

This research did not receive any specific grant from funding agencies in the public, commercial, or not-for-profit sectors.

6. Acknowledgements

We want to thank the CIDNA from Escuela Superior Politécnica del Litoral (ESPOL), for the support during the research process.

References

Avula, S. K., Rehman, N. U., Khan, F., Ullah, O., Halim, S. A., Khan, A., Anwar, M. U., Rahman, S. M., Csuk, R., and Al-Harrasi, A. (2023). Triazole-tethered boswellic acid derivatives against breast cancer: Synthesis, in vitro, and in-silico studies. *Journal of Molecular Structure*, 1282:135181.

Corso, G., Stärk, H., Jing, B., Barzilay, R., and Jaakkola, T. (2022). DiffDock: Diffusion Steps, Twists, and Turns for Molecular Docking. (Figure 1):1–33.

Eastman, P., Swails, J., Chodera, J. D., Mcgibbon, R. T., Zhao, Y., Beauchamp, K. A., Wang, L.-p., Simmonett, A. C., Harrigan, M. P., Stern, C. D., Wiewiora, R. P., Brooks, B. R., and Pande, V. S. (2017). OpenMM 7 : Rapid development of high performance algorithms for molecular dynamics. pages 1–17.

Eberhardt, J., Santos-Martins, D., Tillack, A. F., and Forli, S. (2021). AutoDock Vina 1.2.0: New Docking Methods,

Expanded Force Field, and Python Bindings. *Journal of Chemical Information and Modeling*, 61(8):3891–3898.

Elmorsy, M. R., Abdel-Latif, E., Gaffer, H. E., Mahmoud, S. E., and Fadda, A. A. (2023). Anticancer evaluation and molecular docking of new pyridopyrazolo-triazine and pyridopyrazolo-triazole derivatives. *Scientific Reports*, 13(1):1–17.

Friesner, R. A., Banks, J. L., Murphy, R. B., Halgren, T. A., Klicic, J. J., Mainz, D. T., Repasky, M. P., Knoll, E. H., Shelley, M., Perry, J. K., Shaw, D. E., Francis, P., and Shenkin, P. S. (2004). Glide: A New Approach for Rapid, Accurate Docking and Scoring. 1. Method and Assessment of Docking Accuracy. *Journal of Medicinal Chemistry*, 47(7):1739–1749.

Gorgulla, C., Boeszoermenyi, A., Wang, Z. F., Fischer, P. D., Coote, P. W., Padmanabha Das, K. M., Malets, Y. S., Radchenko, D. S., Moroz, Y. S., Scott, D. A., Fackeldey, K., Hoffmann, M., Iavniuk, I., Wagner, G., and Arthanari, H. (2020). An open-source drug discovery platform enables ultra-large virtual screens. *Nature*, 580(7805):663–668.

Horton, J. R., Liu, X., Gale, M., Wu, L., Shanks, J. R., Zhang, X., Webber, P. J., Bell, J. S., Kales, S. C., Mott, B. T., Rai, G., Jansen, D. J., Henderson, M. J., Urban, D. J., Hall, M. D., Simeonov, A., Maloney, D. J., Johns, M. A., Fu, H., Jadhav, A., Vertino, P. M., Yan, Q., and Cheng, X. RCSB PDB - 5IVE: Linked KDM5A Jmj Domain Bound to the Inhibitor N8 (5-methyl-7-oxo-6-(propan-2-yl)-4,7-dihydropyrazolo[1,5-a]pyrimidine-3-carbonitrile). Available from https://www.rcsb.org/structure/5ive.

Horton, J. R., Liu, X., Gale, M., Wu, L., Shanks, J. R., Zhang, X., Webber, P. J., Bell, J. S., Kales, S. C., Mott, B. T., Rai, G., Jansen, D. J., Henderson, M. J., Urban, D. J., Hall, M. D., Simeonov, A., Maloney, D. J., Johns, M. A., Fu, H., Jadhav, A., Vertino, P. M., Yan, Q., and Cheng, X. (2016). Structural Basis for KDM5A Histone Lysine Demethylase Inhibition by Diverse Compounds. *Cell Chemical Biology*, 23(7):769–781.

Hunter, J. D. (2007). Matplotlib: A 2d graphics environment. *Computing in Science & Engineering*, 9(3):90–95.

Jose, A., Shenoy, G. G., Rodrigues, G. S., Kumar, N. A., Munisamy, M., Thomas, L., Kolesar, J., Rai, G., Rao, P. P., and Rao, M. (2020). Histone demethylase KDM5B as a therapeutic target for cancer therapy. *Cancers*, 12(8):1–16.

Jumper, J., Evans, R., Pritzel, A., Green, T., Figurnov, M., Ronneberger, O., Tunyasuvunakool, K., Bates, R., Žídek, A., Potapenko, A., Bridgland, A., Meyer, C., Kohl, S. A., Ballard, A. J., Cowie, A., Romera-Paredes, B., Nikolov, S., Jain, R., Adler, J., Back, T., Petersen, S., Reiman, D., Clancy, E., Zielinski, M., Steinegger, M., Pacholska, M., Berghammer, T., Bodenstein, S., Silver, D., Vinyals, O., Senior, A. W., Kavukcuoglu, K., Kohli, P., and Hassabis, D. (2021). Highly accurate protein structure prediction with AlphaFold. *Nature*, 596(7873):583–589.

Jurutka, P. W., Di Martino, O., Reshi, S., Mallick, S., Sabir, Z. L., Staniszewski, L. J., Warda, A., Maiorella, E. L., Minasian, A., Davidson, J., Ibrahim, S. J., Raban, S., Haddad, D., Khamisi, M., Suban, S. L., Dawson, B. J., Candia, R., Ziller, J. W., Lee, M. Y., Liu, C., Liu, W., Marshall, P. A., Welch, J. S., and Wagner, C. E. (2021). Modeling, synthesis and biological evaluation of potential retinoid-x-receptor (Rxr) selective agonists: Analogs of 4-[1-(3,5,5,8,8-pentamethyl-5,6,7,8-tetrahyro-2-naphthyl)ethynyl]benzoic acid (bexarotene) and 6-(ethyl(4- isobutoxy-3-isopropylphenyl)amino)nicotinic acid (net-4ib). *International Journal of Molecular Sciences*, 22(22).

Kumar, G., Kumar, P., Soni, A., Sharma, V., and Nemiwal, M. (2024). Efficient synthesis and molecular docking analysis of quinazoline and azole hybrid derivatives as promising agents for anti-cancer and anti-tuberculosis activities. *Journal of Molecular Structure*, 1310(April):138289.

Li, C.-Y., Wang, W., Leung, C.-H., Yang, G.-J., and Chen, J. (2024). KDM5 family as therapeutic targets in breast cancer: Pathogenesis and therapeutic opportunities and challenges. *Molecular Cancer*, 23(1):109.

Ltd2023, E. Screening Collections - Enamine. Available from https://enamine.net/compound-collections/screening-collection.

Nelson, M. J. and Hoover, A. K. (2020). Notes on Using Google Colaboratory in AI Education. *Annual Conference on Innovation and Technology in Computer Science Education, ITiCSE*, pages 533–534.

O'Boyle, N. M., Banck, M., James, C. A., Morley, C., Vandermeersch, T., and Hutchison, G. R. (2011). Open Babel. *Journal of Cheminformatics*, 3(33):1–14.

Ortiz, G., Longbotham, J. E., Qin, S. L., Zhang, M. Y., Lee, G. M., Neitz, R. J., Kelly, M. J., Arkin, M. R., and Fujimori, D. G. (2023). Identifying ligands for the PHD1 finger of KDM5A through high-throughput screening. *RSC Chemical Biology*, 5(3):209–215.

Ramsundar, B., Eastman, P., Walters, P., Pande, V., Leswing, K., and Wu, Z. (2019). *Deep Learning for the Life Sciences*. O'Reilly Media. https://www.amazon.com/Deep-Learning-Life-Sciences-Microscopy/dp/1492039837.

RDKit, online. RDKit: Open-source cheminformatics. http://www.rdkit.org. [Online; accessed 11-April-2013].

Rose, A. S., Bradley, A. R., Valasatava, Y., Duarte, J. M., Prlic, A., and Rose, P. W. NGL viewer: Web-based molecular graphics for large complexes. *Bioinformatics*, (21):3755–3758.

Schmitt, M. and Greten, F. R. The inflammatory pathogenesis. *Nature Reviews Immunology*, 0123456789.

Senior, A. W., Evans, R., Jumper, J., Kirkpatrick, J., Sifre, L., Green, T., Qin, C., Žídek, A., Nelson, A. W., Bridgland, A., Penedones, H., Petersen, S., Simonyan, K., Crossan, S., Kohli, P., Jones, D. T., Silver, D., Kavukcuoglu, K., and Hassabis, D. (2020). Improved protein structure prediction using potentials from deep learning. *Nature*, 577(7792):706–710.

Sliwoski, G., Kothiwale, S., Meiler, J., and Lowe, E. W. (2014). Computational methods in drug discovery. *Pharmacological Reviews*, 66(1):334–395.

Van Rossum, G. and Drake Jr, F. L. (1995). *Python tutorial*. Centrum voor Wiskunde en Informatica Amsterdam, The Netherlands.

Yang, G. J., Ko, C. N., Zhong, H. J., Leung, C. H., and Ma, D. L. (2019). Structure-based discovery of a selective KDM5A inhibitor that exhibits anti-cancer activity via inducing cell cycle arrest and senescence in breast cancer cell lines. *Cancers*, 11(1):1–15.